NASA Contractor Report 201606

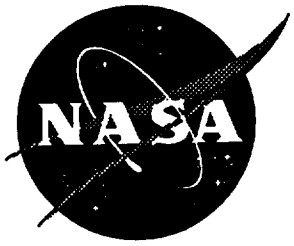

Computational Study of a McDonnell Douglas Single-Stage-to-Orbit Vehicle Concept for Aerodynamic Analysis

Ramadas K. Prabhu
Lockheed Martin Engineering & Sciences Company, Hampton, Virginia

Contract NAS1-19000

September 1996

National Aeronautics and
Space Administration
Langley Research Center
Hampton, Virginia 23681-0001

Computational Study of a McDonnell Douglas Single-Stage-to-Orbit Vehicle Concept for Aerodynamic Analysis

Ramadas K. Prabhu
Lockheed Martin Engineering & Sciences Company
Hampton, VA 23666

Summary

This paper presents the results of a computational flow analysis of the McDonnell Douglas single-stage-to-orbit vehicle concept designated as the 24U. This study was made to determine the hypersonic aerodynamic characteristics of the vehicle with and without body flaps over an angle of attack range of 20-40 deg. Computations were made at a flight Mach number of 20 at 200,000 ft. altitude with equilibrium air, and a Mach number of 6 with CF_4 gas. The software package FELISA (Finite Element Langley Imperial College Swansea Ames) was used for all the computations. The FELISA software consists of unstructured surface and volume grid generators, and inviscid flow solvers with (1) perfect gas option for subsonic, transonic, and low supersonic speeds, and (2) perfect gas, equilibrium air, and CF_4 options for hypersonic speeds. The hypersonic flow solvers with equilibrium air and CF_4 options were used in the present studies. Results are compared with other computational results and hypersonic CF_4 tunnel test data.

Symbols

AF	Axial force, N
A_{ref}	Reference area, m^2
$C_A=AF/(A_{ref}q_\infty)$	Axial force coefficient
$C_N=NF/(A_{ref}q_\infty)$	Normal force coefficient
$C_M=PM/(A_{ref}d_{ref}q_\infty)$	Pitching moment coefficient
$C_p=(p-p_\infty)/q_\infty$	Pressure coefficient
d_{ref}	Reference length for pitching moment, m
M	Mach number
NF	Normal force, N
p	Static pressure, N/m^2
PM	Pitching moment about the reference point, Nm

$q_\infty = \rho_\infty V^2_\infty/2$	Freestream dynamic pressure, N/m^2
r, R	Distances associated with a source, m (see page 4)
T_∞	Freestream static temperature, K
V_∞	Freestream velocity, m/s
x	Distance along the body axis, measured from the nose, m
α	Angle of attack, deg.
δ_1	Minimum spacing due to a point source, m (see page 4)
$\delta(x)$	Grid spacing at a distance x from a point source, m
δ_{bf}	Body flap deflection angle, deg.
δ_{yf}	Yaw flap deflection angle, deg.
ρ_∞	Freestream density, kg/m^3

Subscripts

ref	reference quantity
bf	Body flap
yf	Yaw flap
∞	Freestream

Introduction

The objective of this study is to determine the effectiveness of the body flap on the McDonnell Douglas 24U configuration (sketch is shown in Fig. 1). This body is symmetric about the *x*-*z* plane; hence only one half of the body is modeled in the present computations. The body has a hemispherical nose, followed by a conical mid-section that transitions into a aft-section with a nearly flat bottom. The body flap is on the underside of this section with its hinge line perpendicular to the symmetry plane. The yaw flap is on the side of the body with its hinge line inclined 35 deg. to the body axis. There are two fixed fins at 45 deg. to the symmetry plane.

Unstructured grids were used for all the computations reported here. Some of the details of the unstructured grid generation process are discussed. In hypersonic equilibrium flows the bow shock in front of a vehicle lies very close to the body. It is important to have adequate grid resolution to capture this bow shock. A method of obtaining grids that capture such shocks, and the solution procedure are described.

Computations were made on the clean configuration (flaps not deflected) and on the deflected flap configurations (δ_{bf}= 20 and δ_{yf}= 15 deg.) with the freestream conditions that correspond to Mach 20 flight at 200,000 ft. altitude. An angle of attack range of 20 to 40 deg. was covered. The unstructured surface and volume grid generator and hypersonic solver from FELISA, with equilibrium air option, were used for all the computations at Mach 20.

The Langley hypersonic CF_4 tunnel (Ref. 1) is a blow-down tunnel that employs carbon tetrafluoride as the test gas. The purpose of this tunnel is to provide a conventional test environment that simulates real-gas effects that occur in hypersonic atmospheric flight (see Ref. 2). For hypersonic atmospheric flight, normal shock density ratios of 10-20 may be reached, as compared to a ratio of 6 for ideal gas air. Use of CF_4 as the test gas in a conventional blow-down type wind tunnel provides a testing environment with a normal shock density ratio of 12, simulating the flow conditions over a vehicle in hypervelocity atmospheric flight. The Langley hypersonic CF_4 (Mach 6) tunnel has been successfully used to simulate hypersonic flow past the Space Shuttle Orbiter (Ref. 3) and the Aeroassist Flight Experiment (AFE) configuration (Ref. 4). The 24U body was tested in the Langley hypersonic CF_4 tunnel to determine its aerodynamic characteristics with and without the flaps. In order to simulate these tests, the FELISA solver was modified by replacing the equilibrium air properties with CF_4 gas properties, and was run with the tunnel test conditions for the freestream.

Present results with the equilibrium air option are compared with similar results obtained independently by McDonnell Douglas using FELISA software. The present results with the CF_4 gas option are compared with experimental data from hypersonic CF_4 tunnel tests. Generally there is a good agreement between computations and test data. However, some significant differences are noticed between the equilibrium air results at Mach 20 and the CF_4 results at Mach 6 for α=40 deg. Possible causes of these differences are discussed.

Unstructured Grid Generation

Designing an unstructured grid that captures the important features of a hypersonic flowfield is a challenging task. Adaptive remeshing is often employed for this purpose. This process consists of starting with a relatively coarse grid, computing the flow on that grid, and using that information to determine the nodal spacings in the adapted grid. Such an adaptive remeshing procedure generally leads to a grid with small nodal spacings in regions of high gradients. In a hypersonic flowfield, however, the gradient of flow variables can vary over a wide range. In such a case, the adaptive remeshing technique often fails to produce satisfactory grids. Other procedures that enhance grid quality could be used. For example, mesh movement based on the gradients of a selected flow quantity is possible, but the benefits from this procedure are small. Mesh enrichment is another possible means of mesh enhancement. However, the user has to be

very cautious in using this technique; more often than not this approach results in extremely large grids.

In the present study, remeshing is not attempted, and mesh enhancements, namely, mesh movement and enrichment are also not applied. All the computations are made on well designed grids obtained by the proper choice of the grid spacings. It was necessary to exercise extreme care in generating these grids, so that flow features are well captured; at the same time, the mesh sizes are kept within reasonable limits.

An important part of the grid generation process is setting the nodal spacings in the computational domain so that an optimal grid suitable for the given problem is obtained. In the FELISA surface and volume grid generation process, the nodal spacings are determined by a number of point, line, and triangle sources placed in the background grid. Determining the number, the numerical values for the parameters δ_1, r, and R, and the location for placing these sources in the background grid is a major task.

The grid spacing $\delta(x)$ at a distance x from a point source is given by the following relation:

$$\delta(x) = \delta_1, \text{ if } x < r$$

$$= \delta_1 \exp[\, |(x-r)/(R-r)| \log(2) \,], \text{ if } x > r$$

This function provides a uniform grid spacing within a sphere of radius r centered at the source, and a rapidly increasing grid spacing away from it. The grid spacings due to line and triangle sources are given by similar expressions. It should be emphasized here that properties of the sources should be chosen with care. Fine spacing could result in an unduly large grid that could take too much of the computational resources, whereas coarse spacing could lead to a grid that would result in poor quality solution; in some cases such coarse grids might not work. An exhaustive description of the sources and the unstructured grid generation process may be found in the FELISA Reference Manual (Ref. 5).

One of the areas in the computational domain that requires special consideration during the grid generation for slender bodies in hypersonic flows is the nose region. In hypersonic flows the bow shock stand-off distance for a body with a hemispherical nose is very small. For example, at Mach 20 in perfect gas air, the shock stand-off distance is about 14% of the nose radius. The shock stand-off distance in equilibrium air or in CF_4 is even smaller (8% of the nose radius). It is very important to capture this bow shock well. Further, it is necessary to place about 10 to 12 points between the bow shock and the body so that the flow in the shock layer is well resolved. Away from the stagnation point, the distance between the body and the shock increases and, hence, relatively larger spacing may be used away from the stagnation point.

The required grid spacing around the nose is obtained by placing a sufficiently large number of point sources on the hemispherical nose. The properties of these sources (δ_1, r, and R)

are chosen so that near the stagnation point the values of δ_1, r, and R are the least. Generally, δ_1 is chosen to be 1/15 to 1/20 of the shock stand-off distance, r to be 1.2 times the shock stand-off distance, and R to be 1.5 times r. For the point sources away from the stagnation point, the values of δ_1, r, and R are increased gradually.

Choosing the location and appropriate values for the source parameters requires a prior knowledge of the shock location around the body. Therefore, the first step is to solve the problem on a grid having a relatively coarse spacing, and to determine an approximate location for the bow shock and other flow features. The shock stand-off distance from this exercise should suffice in determining the spacing (the point source properties) around the nose. The solution on the coarse grid is also useful in setting the spacings required elsewhere in the computational domain. For example, a fine grid spacing is required to capture the (oblique) shock generated at the leading edge of a deflected flap. Further, the solution on the coarse grid can be used to interpolate on to the fine grid, which will save some computational time on the fine grid.

Figure 2 shows a typical grid in front of the nose on the plane of symmetry. Over 400 point sources were distributed on the hemispherical surface to generate this grid. A simple FORTRAN code was written to generate the location and the properties of these sources. Figure 3 shows a part of the grid on the plane of symmetry near the deflected flap. Notice the dense grid designed to capture the oblique shock from the leading edge of the deflected flap.

Flow Solver

The FELISA inviscid hypersonic flow solver algorithm is based on the Haenel flux vector splitting technique (Ref. 6). More information on the solution algorithm may be found in Bibb, et al. (Ref. 7). As noted earlier, the scheme conserves total enthalpy and assumes the working medium to be a perfect gas.

At very high temperatures encountered in hypersonic atmospheric flight, the perfect gas assumption is not valid. Therefore, extensive changes were made to the solver, and the perfect gas relations were replaced with equilibrium air relations. Tannehill's curve fits (Ref. 8) were used for this purpose. Corresponding changes were also made to related post-processing codes. In order to investigate the differences between the FELISA computational results with equilibrium air and CF_4 tunnel data, the FELISA hypersonic solver was run with CF_4 as the working gas. For this purpose the solver was modified by replacing Tannehill's curve fits for equilibrium air properties with simpler algebraic equations for the CF_4 gas properties derived by Sutton (Ref. 9). Similar changes were made in all the post-processing codes as well.

Solution Procedure

Initially, the solver was run with the lst-order option at a Courant number of 0.6 for 500 steps. Next, the higher order option was turned on, and the solver was run to convergence with a CFL number of about 0.3. Well designed grids lead to faster convergence. The residuals and the maximum and minimum total enthalpies in the flow field were tracked though these iterations. The integrated quantities, namely the axial and normal forces and the pitching moment, were also tracked. When the integrated quantities reach steady values, which took typically 800 to 1000 higher order steps, the solution was assumed to be converged. At this point some differences between the maximum and minimum total enthalpies might be present. It should be noted that the solution algorithm preserves total enthalpy in the computational domain. Subsequent iterations drive the total enthalpy variations towards zero; however, these iterations do not lead to any significant changes in the integrated quantities.

Results and Discussion

Flap Effectiveness Studies in Equilibrium Air:

For all the computations made on the 24U body to determine its aerodynamic characteristics assuming equilibrium air, the freestream conditions were as follows:

Velocity (V_∞) = 6377 m/s

Temperature (T_∞) = 253 K

Density (ρ_∞) = 2.5109E-4 kg/m^3

These conditions correspond to a flight Mach number of 20 at an altitude of 200,000 ft. The forces and moments were non-dimensionalized in the standard way using the following reference quantities:

Ref. area (A_{ref}) = 49.803 m^2 (=77,195 sq. in.) equal to the body cross-sectional area at the end of the conical section

Ref. length (d_{ref}) = 28.499 m (=1,122 in.) equal to the body length

Ref. point for C_M = 19.379 m (=762.96 in.) aft of nose on the body axis (68% of the body length behind the nose)

The results of this study are summarized in Table 1, and are shown graphically in Figs. 4-6. It should be noted that the force and moment coefficients are for the forebody only, and do not include the contributions from the base. Similar computations were made independently by McDonnell Douglas on the same configuration using the FELISA equilibrium air code but using entirely different grids. Their results (referred to as MDC) are also shown in Figs. 4-6. It is gratifying to note that MDC results agree well with the present computations.

It should be noted that the present computations assume inviscid flow. The effect of viscosity on the aerodynamics of slender bodies is primarily on the axial force. Inviscid computations underpredict the axial force because of the absence of skin friction. Also, flow

separations on the body could alter the pressure distribution, leading to changes in normal force and pitching moment. However, on a slender body like the 24U, there are not likely to be any significant flow separations up to α=40 deg. Hence, it is expected that the present inviscid computations would predict accurate values of normal force and pitching moment.

The flaps are located on the aft section of the vehicle. Deflection of these flaps do not have any significant influence on the pressure distribution on other parts of the body. Hence, the contribution to aerodynamic loads due to flap deflection can be easily isolated.

Variation of axial force coefficient, C_A, with α is shown in Fig. 4. As expected, deflection of the body flap by 20 deg. increases the C_A significantly. This increment increases from 0.186 at α = 20 deg. to 0.323 at α = 40 deg. Deflection of the yaw flap by 15 deg. also increases C_A, but this increase is relatively small (δC_A = 0.020) and is the same at α = 30 and 40 deg.

Variation of normal force coefficient, C_N, with α is shown in Fig. 5. The body flap deflection increases the normal force coefficient significantly. Upon close examination, it can be observed that the increment in the normal force coefficient due to the body flap deflection increases from 0.409 at α = 20 deg. to 0.615 at α= 30 deg., and then decreases to 0.556 at α= 40 deg. Deflection of the yaw flap by 15 deg. also increases C_N, but this increase, as in the case of axial force, is relatively small (δC_N= 0.013), and appears to be the same for α = 30 and 40 deg.

Variation of pitching moment coefficient, C_M, with α is shown in Fig. 6. The 20 deg. body flap deflection results in a large nose down pitching moment. This nose down pitching moment increment increases from -0.147 at α= 20 deg. to -0.208 at α= 30 deg. and then drops to -0.193 at α = 40 deg. This trend is consistent with the observed trend in the normal force coefficient. The cause of this becomes clear when we examine the flow on and around the flap in one of the following sections. As before, the contribution due to the yaw flaps is small (δC_M = 0.0036).

Flap Effectiveness Studies in CF_4:

The 24U body was tested in the Langley hypersonic CF_4 tunnel to determine the contribution to C_N and C_M from the body flap deflected by 25 deg. It was expected that these test results would be representative of the aerodynamic data of the vehicle in hypersonic flight. In order to simulate these tests, computations were made on the 24U body at a nominal Mach number of 6 with CF_4 gas instead of equilibrium air. The freestream conditions for these computations were as follows:

Velocity (V_∞)	= 842.3 m/s
Temperature (T_∞)	= 166 K
Density (ρ_∞)	= 1.739E-2 kg/m^3

These conditions correspond to those in the Langley hypersonic CF_4 tunnel during the tests on the 24U body. Computations were made at three different angles of attack, with and without the flap

deflection. The results are summarized in Table 2, and shown graphically in Figs. 7 and 8. Results from the hypersonic CF_4 tunnel tests on a 24U model are also included in these figures. The reference area and length, and the pitching moment reference point for these results are the same as in the case of the equilibrium air. As in the case of equilibrium air computations, the force and moment coefficients are for the forebody only (i.e., do not include base effects).

It should be emphasized that the present computations assume inviscid flow. Hence, no attempt has been made to compare computed axial force coefficients with those measured in the CF_4 tunnel tests. The effect of viscosity is to introduce skin friction, thereby increasing the axial force. Flow separation due to viscous effects would affect the pressure distribution on the body, thereby affecting the loads on the body. But, as noted earlier, for a slender body like the 24U, there is no likelihood of significant separation up to moderate angles of attack (40 deg.). Hence, it is expected that inviscid computations would predict the normal force and the pitching moment with good accuracy.

Variation of the computed normal force coefficient, C_N, with α is shown in Fig. 7 for clean (δ_{bf} =0, δ_{yf} =15 deg.), as well as for the body flap deflected (δ_{bf} =20, δ_{yf} =15 deg.), cases. Experimental data from the CF_4 tunnel tests are also shown in the figure. The computed C_N values seem to be consistently higher than the experimental data by about 5% for the clean, as well as flap deflected, cases; thus, the computed values of C_N due to body flap deflection are judged to be in good agreement with the experimental data. Unlike the equilibrium air case, this value seems to steadily increase with the angle of attack up to α = 40 deg. The effect of deflecting the yaw flap by 15 deg. is to increase the C_N by approximately 0.033.

Variation of the computed pitching moment coefficient, C_M, with α is shown in Fig. 8, along with the CF_4 tunnel test data. There is a good agreement between the computed results and the CF_4 tunnel test data. An interesting observation in this figure is that the body is unstable when the body flap is not deflected; however, when the body flap is deflected by 20 deg., the body becomes neutrally stable (slope of C_M vs. α curve is zero). Unlike the equilibrium air case, contribution of the deflected flap to C_M increases steadily with angle of attack through α = 40 deg. This is consistent with the observed behavior in the C_N. Deflection of the yaw flap by 15 deg. causes a nose down pitching moment of approximately 0.0094.

Discussion:

The equilibrium air computations for the 24U body predict that the normal force due to the body flap deflection increases up to α=30 deg. and then decreases somewhat. The pitching moment also exhibits a similar trend. Such a drop in the normal force due to the flap deflection is not observed either in the CF_4 computational results or in the CF_4 tunnel test data. This is an unexpected result. In the past, computations with CF_4 gas gave good agreement with measurements for the Space Shuttle Orbiter (Ref. 3) and the AFE body (Ref. 4).

The primary cause of the differences in the equilibrium air and CF_4 results can be traced to the differences in the flow about the deflected flap. Figures 9, 10, and 11 show pressure contours on the plane of symmetry near the deflected flap for α = 20, 30, and 40 degrees, respectively. It may be seen in these figures that for a given angle of attack, the bow shock originating at the nose is closer to the body for equilibrium air than for CF_4. The shock stand-off distance for a given body is determined primarily by the density ratio behind the shock. The normal shock density ratio at the nose region was found to be about 15.3 for equilibrium air compared to a value of about 11.8 for the CF_4. This causes the bow shock in front of the nose to lie closer to the surface for the equilibrium air case. Similarly, the density ratio in front of the oblique shock due to the flap for equilibrium air is 9 compared to a value of 7 for the CF_4 case (See Figures 12). The higher density ratio across the bow shock in the region upstream of the flap causes the shock to lie closer to the surface for the equilibrium air case compared to the CF_4 case.

The bow shock interacts with the oblique shock originating from the leading edge of the deflected flap (as shown in Figs. 9-11), leading to complex flow patterns (See, e.g., Ref. 10). If flow from the shock interaction impinges on the flap, then the pressure distribution on the flap is dramatically changed. For CF_4, at angles of attack up to 30 deg. the bow shock detachment distance is sufficiently large to avoid a shock interaction in the vicinity of the flap. However, since the bow shock is closer to the body for equilibrium air, the shock interaction occurs in the immediate vicinity of the flap, and the resulting flow affects the pressure distribution on the flap.

As the angle of attack is increased from 20 to 40 deg., the bow shock moves progressively closer to the body in both CF_4 and equilibrium air cases. Again, the shock is further away from the body for the CF_4 case compared to the equilibrium air case. In both cases, the bow shocks intersect the oblique shocks caused by the flap, and the complex flows resulting from these shock interactions affect the flow on the flaps. However, in the equilibrium air case, a much larger area of the flap is affected by the interaction for a given angle of attack.

The computed C_p distribution on the body at the symmetry plane for both Mach 20 equilibrium air and Mach 6 CF_4 are shown in Figs. 13-15. The C_p distribution on the flap ($x >$ 1000 in) shows a peak close to the hinge line. Peaks in the C_p distribution in the vicinity of the hinge lines have been observed experimentally, and viscous flow computations have successfully reproduced such results. The origin for such a peak lies in the flow separation ahead of the flap hinge line, and subsequent flow reattachment. The present computations are inviscid, and the source of the pressure peak in the present results is not clear.

At α = 20 deg. the C_p distribution on the flap center line for CF_4 (Fig. 13) is nearly constant, whereas for equilibrium air, C_p increases towards the trailing edge of the flap. This rise is partly due to the fact that the flow approaching the flap is not uniform. It is also a characteristic

of the flow resulting from shock interactions. The average pressure on the flap is greater in equilibrium air than in CF_4.

At $\alpha = 30$ deg. the effect of the shock interaction can be clearly seen for the equilibrium air case; the C_p rises sharply, and then drops to a low value at the flap trailing edge (see Fig. 14). Such a peak is not seen for the CF_4 case, suggesting that the shock interaction is not affecting the pressures on the flap surface.

At $\alpha = 40$ deg. the C_p distribution for CF_4 (Fig. 15) has a peak close to the flap trailing edge, indicative of the influence of a shock interaction. The peak in the C_p distribution for the equilibrium air case has moved much closer to the flap leading edge. This is a result of the shock interaction occurring closer to the body. This leads to loss of normal force due to the flap and reduced flap effectiveness. These inferences fully concur with the earlier observation made by examining the pressure contours.

As previously cited, high quality aerodynamic data for the Space Shuttle Orbiter and the AFE body were obtained in the hypersonic CF4 tunnel. Both of these bodies are blunt compared to the 24U. Hence, the shock stand-off distances for these bodies are larger compared to the shock stand-off distance for the 24U. This, combined with only a 16 deg. flap deflection on the Space Shuttle Orbiter, mitigated possible shock interaction in the earlier computations on the Space Shuttle Orbiter. In the present case the 24U has a slender body, and the flap deflection considered is 20 deg. These factors led to shock interaction, and a loss of effectiveness of the flap at α=40 deg.

Conclusion

Computations were made on the McDonnell Douglas single-stage-to-orbit vehicle designated as the 24U to determine the aerodynamic characteristics with and without the body flap for Mach 20 flight conditions assuming equilibrium air. Similar computations were made assuming CF_4 gas, and the freestream corresponding to the Langley hypersonic CF_4 (Mach 6) tunnel test conditions. The computed equilibrium air results compared well with other similar computational results, and the computed CF_4 results compared well with hypersonic CF_4 tunnel test data. Also, there was good agreement between equilibrium air and CF_4 results up to α=30 deg. However, when the angle of attack was increased from 30 to 40 deg., the loads due to the flap deflection dropped in the equilibrium air case, whereas they continued to increase in the CF_4 case.

This difference between equilibrium air and CF_4 computations at α=40 deg. with the body flap deflected 20 deg. is totally unexpected. In the past, CF_4 computations gave good agreement for the Space Shuttle Orbiter as well as the AFE body. Close examination of the computed pressure contours for α=40 deg. near the body flap reveals significant differences in the flow over the deflected flap in the equilibrium air and the CF_4 cases. There is a strong shock interaction in

the equilibrium air case that leads to significant changes in the pressure distribution on the flap. Although there is a shock interaction in the CF_4 case also, it occurs further away from the flap, and the pressure distribution on the flap is not significantly affected. In the earlier computations on the AFE body, there were no such complex flows. The Space Shuttle Orbiter has a blunt nose, which results in a relatively large shock stand-off distance. This large shock stand-off distance, combined with a smaller flap deflection (16 deg.), mitigated the shock interaction on the flap. The 24U is a slender body, causing the shock to lie close to the body, leading to the shock interaction effects.

Acknowledgments

This work was done at Lockheed Martin Engineering & Sciences Company in Hampton, Virginia, and was supported by the Aerothermodynamics Branch, NASA Langley Research Center, under contract NAS1-19000. The author wishes to thank Mr. K. James Weilmuenster and Dr. Kenneth Sutton for many helpful discussions, Mr. William Woods for the hypersonic CF_4 tunnel test data included in this document, and Mr. Scott Ward of McDonnell Douglas for permission to include their FELISA computational results in this document.

References

1. Micol, J. R., Midden, R. E., and Miller, C. G. III: "Langley 20-Inch Hypersonic CF_4 Tunnel: A Facility for Simulating Real-Gas Effects," AIAA-92-3939, January 1992.
2. Jones, Robert A. and Hunt, James L.: "Use of Tetrafluoromethane to Simulate Real-Gas Effects on the Hypersonic Aerodynamics of Blunt Vehicles," NASA TR R-312, 1969.
3. Brauckmann, G. J., Paulson, J. W. Jr., and Weilmuenster, K. J.: "Experimental and Computational Analysis of Shuttle Orbiter Hypersonic Trim Anomaly," *Journal of Spacecraft and Rockets*, Vol. 32, No. 5, September-October 1995, pp. 758-764.
4. Wells, W. L.: "Measured and Predicted Aerodynamic Coefficients and Shock Shapes for Aeroassist Flight Experiment (AFE) Configuration," NASA Technical Paper 2956, January 1990.
5. Peiro, J., Peraire, J., and Morgan, K.: "FELISA System, Reference Manual," August 1994.
6. Haenel, D., Schwane, R., and Seider, G.: "An Implicit Flux Vector Splitting Scheme for the Computation of Viscous Hypersonic Flow," AIAA Paper 89-0274, 1989.
7. Bibb, K. L., Peraire, J., Riley, C. J., and Weilmuenster, K. J.: "Hypersonic Flow Computations on Unstructured Meshes," AIAA Paper 97-0625 (under preparation for presentation at the 35th Aerospace Sciences Conference, Reno, Nevada, January 1997.

8. Srinivasan, S., Tannehill, J. C., and Weilmuenster, K. J.: "Simplified Curve Fits for the Thermodynamic Properties of Equilibrium Air," NASA Reference Publication 1181, August 1987.
9. Sutton, K.: "Relations for the Thermodynamic and Transport Properties in the Testing Environment of the Langley Hypersonic CF_4 Tunnel," NASA Technical Memorandum 83220, October 1981.
10. Olejniczak, J., Wright, M. J., and Candler, G. V.: "Numerical Study of Shock Interactions on Double-Wedge Geometries," AIAA Paper 96-0041, January 1996.

Table 1

SUMMARY OF THE COMPUTED AERODYNAMIC DATA ON THE 24U BODY IN EQUILIBRIUM AIR

Flight Conditions: M_∞= 20 (Nominal), V_∞ = 6377 m/s, T_∞ = 253K, ρ_∞ = 2.5109E-4 kg/m^3

α, deg.	Flap deflections, deg.		C_A	C_N	C_M	Mesh
	(Body)	(Yaw)				
20	0	0	0.294	1.040	0.0770	1
30	0	0	0.384	1.704	0.1282	2
40	0	0	0.463	2.505	0.1600	3
20	20	0	0.480	1.449	-0.0704	4
30	20	0	0.669	2.319	-0.0803	5
40	20	0	0.786	3.061	-0.0331	6
30	0	15	0.402	1.716	-0.1247	7
40	0	15	0.484	2.519	-0.1563	8

NOTES:
1. Reference area = 77,195 sq. in. (equal to the cross-sectional area at the end of the conical part of the body)
2. Reference length = 1,122 in. (equal to the body length)
3. Moment ref. point 762.96 in. aft of nose (on the axis at 68% of the body length behind the nose)
4. Meshes 1, 2, 3, and 6 have over 400K nodes.
5. Meshes 4 and 5 have over 600K nodes.
6. Meshes 7 and 8 have over 490K nodes.
7. C_A, C_N, and C_M values do not include contribution from the base.

Table 2

SUMMARY OF THE COMPUTED AERODYNAMIC DATA ON THE 24U BODY IN CF_4

Test Conditions: M_∞= 6 (Nominal), V_∞ = 842.3 m/s, T_∞ = 166K, ρ_∞ = 1.739E-2 kg/m^3

α, deg.	Flap deflections, deg.		C_A	C_N	C_M	Mesh
	(Body)	(Yaw)				
30	20	0	0.596	2.293	-0.0240	1
40	20	0	0.775	3.180	-0.0231	1
30	0	15	0.398	1.869	0.1233	2
40	0	15	0.492	2.669	0.1589	3
20	20	15	0.445	1.481	-0.0383	4
30	20	15	0.621	2.328	-0.0336	5
40	20	15	0.800	3.211	-0.0323	6

NOTES:
1. The reference quantities are the same as those used for equilibrium air case.
2. Mesh 1 has over 450K nodes.
3. Meshes 2-6 have over 600K nodes.
4. C_A, C_N, and C_M values do not include contribution from the base.

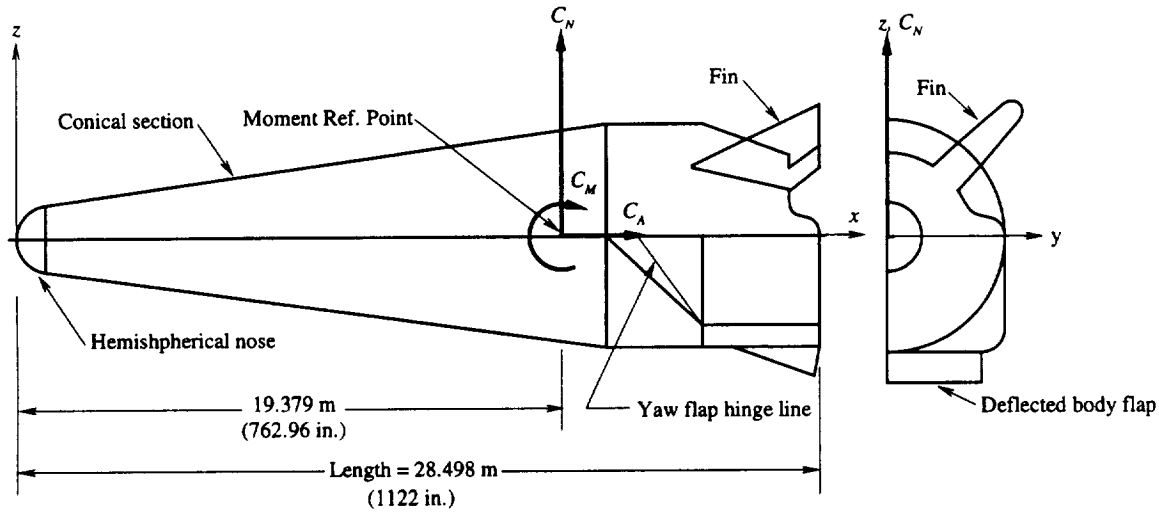

Fig. 1 A sketch showing the 24U body with fin and deflected flap

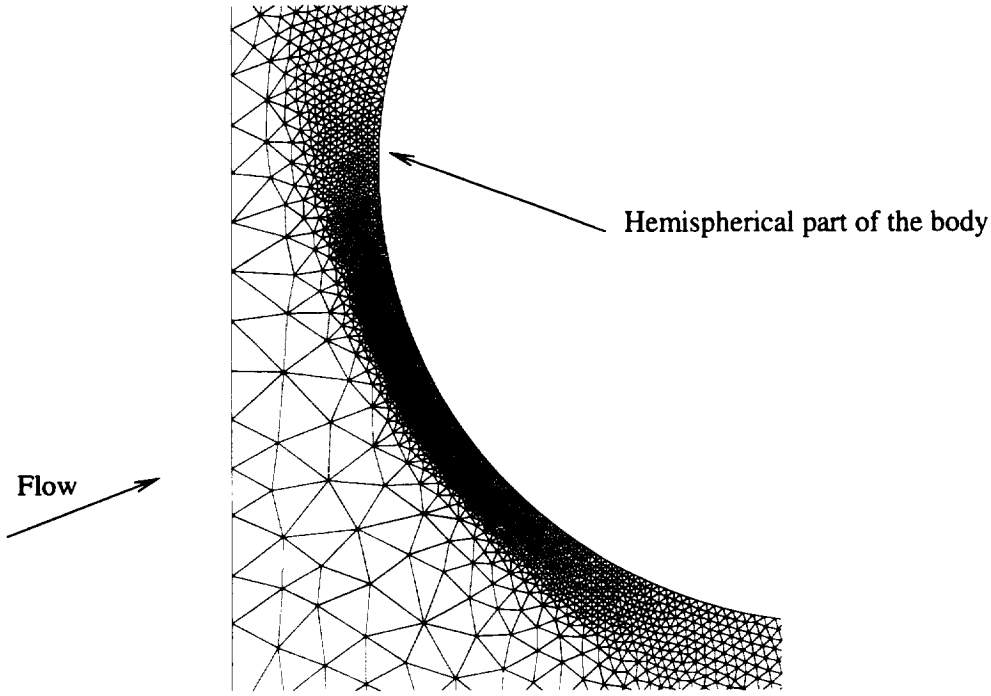

Fig. 2 A part of a typical unstructured grid on the symmetry plane near the stagnation point

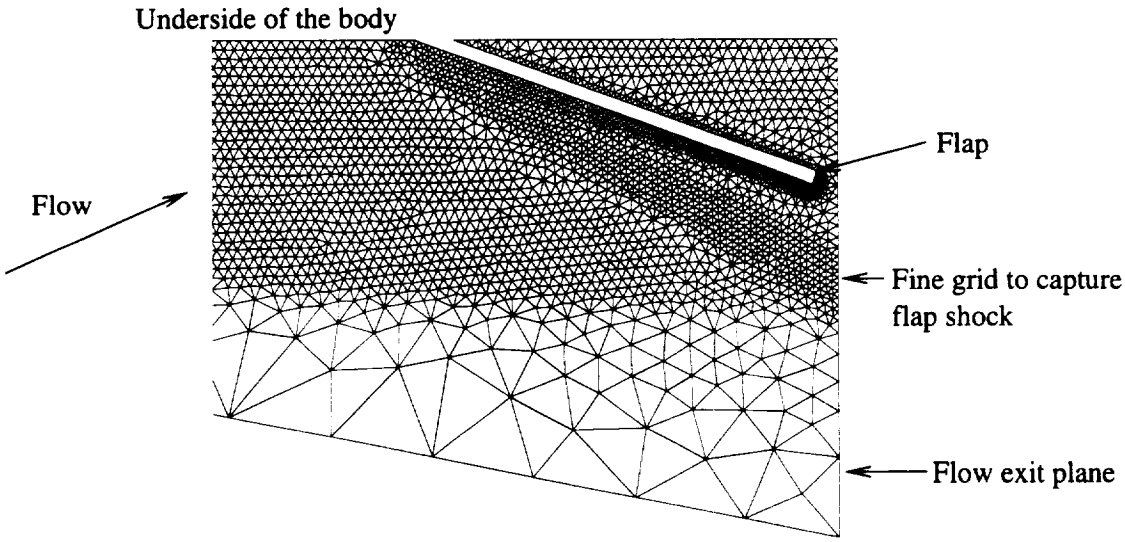

Fig. 3 A part of a typical unstructured grid on the symmetry plane near the deflected flap

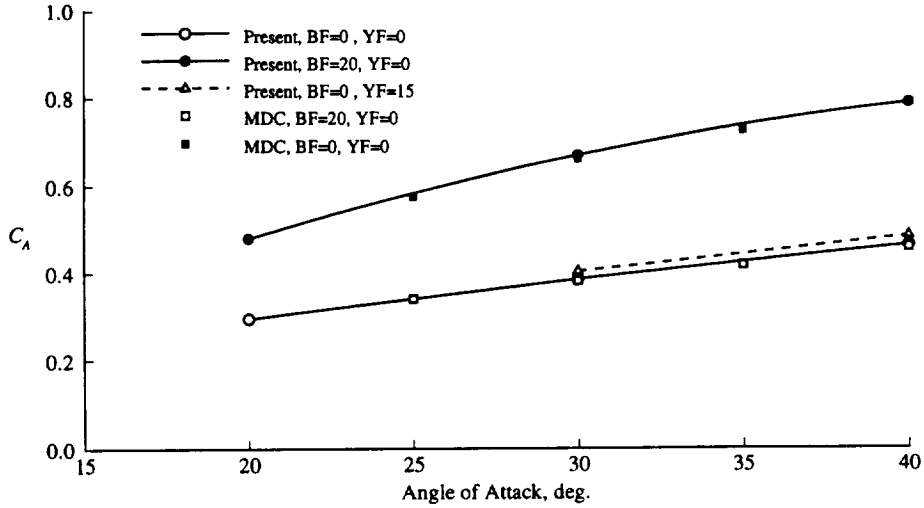

Fig. 4 Variation of axial force coefficient with angle of attack for the 24U at Mach 20 in equilibrium air

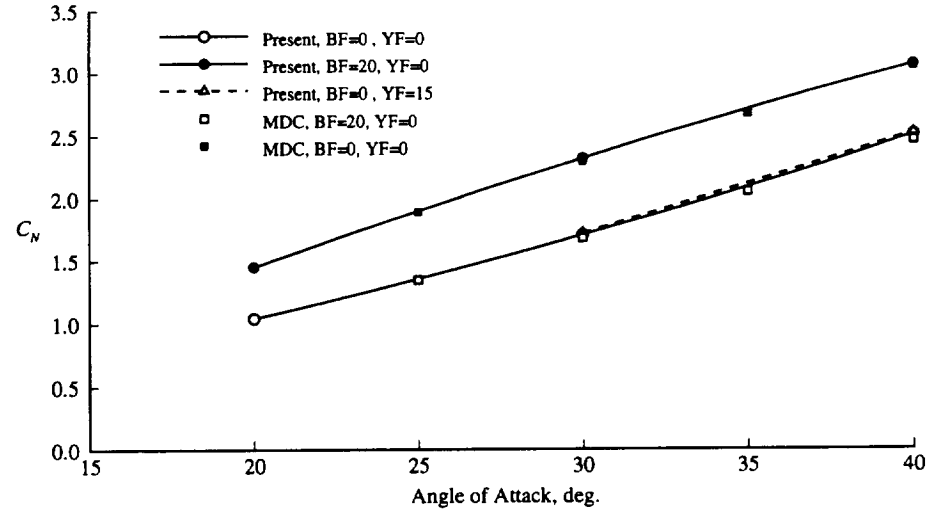

Fig. 5 Variation of normal force coefficient with angle of attack for the 24U at Mach 20 in equilibrium air

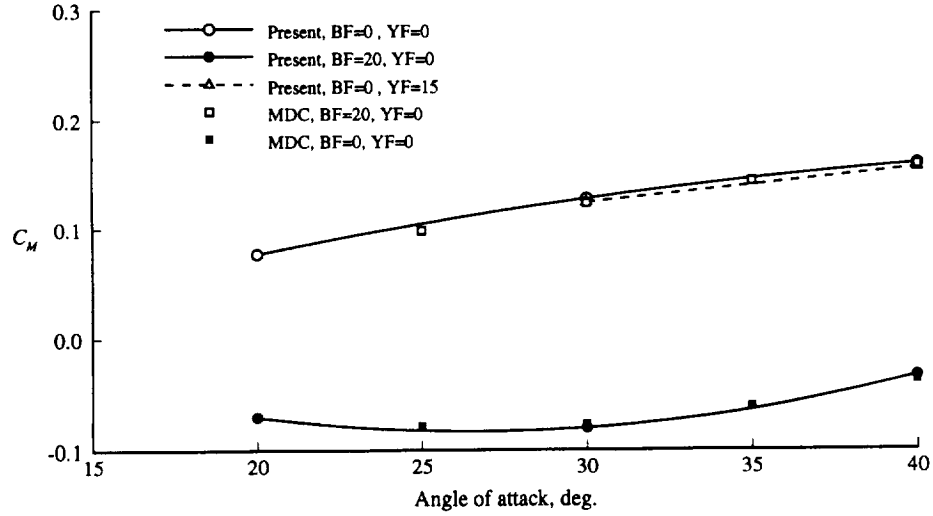

Fig. 6 Variation of pitching moment coefficient with angle of attack for the 24U at Mach 20 in equilibrium air

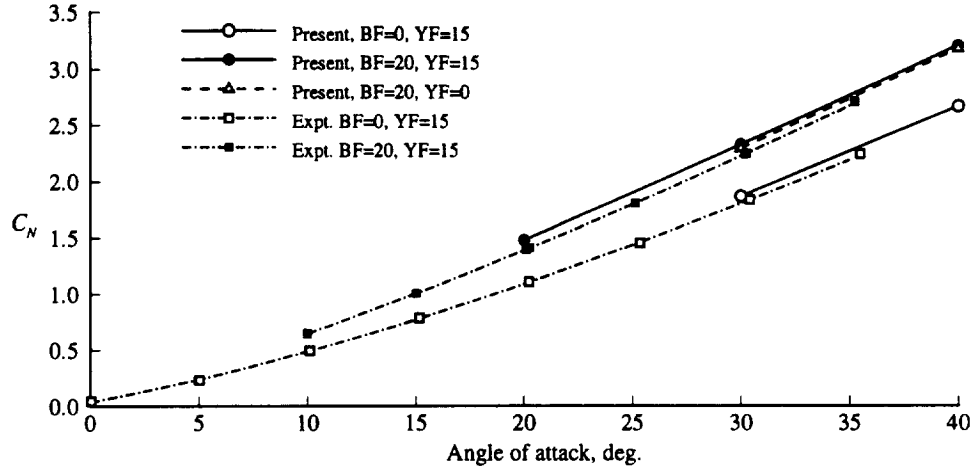

Fig. 7 Variation on normal force coefficient with angle of attack for the 24U at Mach 6 in CF_4

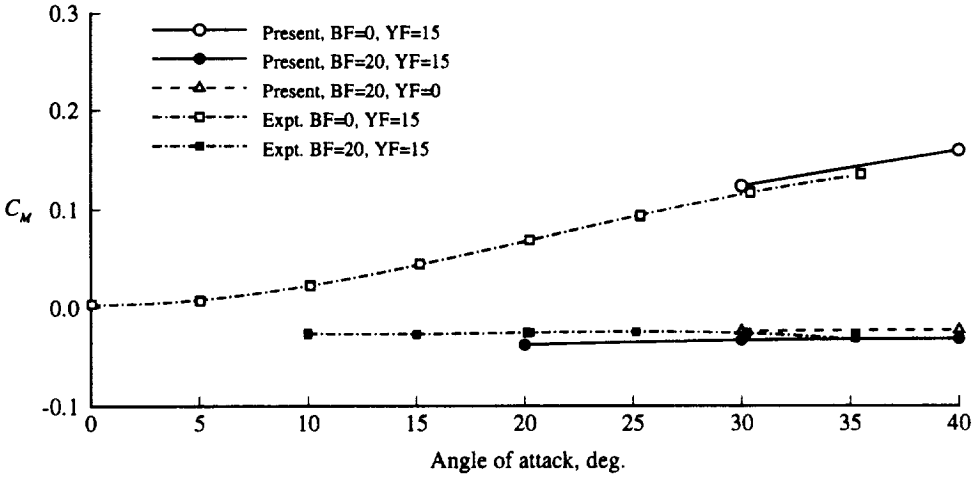

Fig. 8 Variation of pitching moment coefficient with angle of attack for the 24U at Mach 6 in CF_4

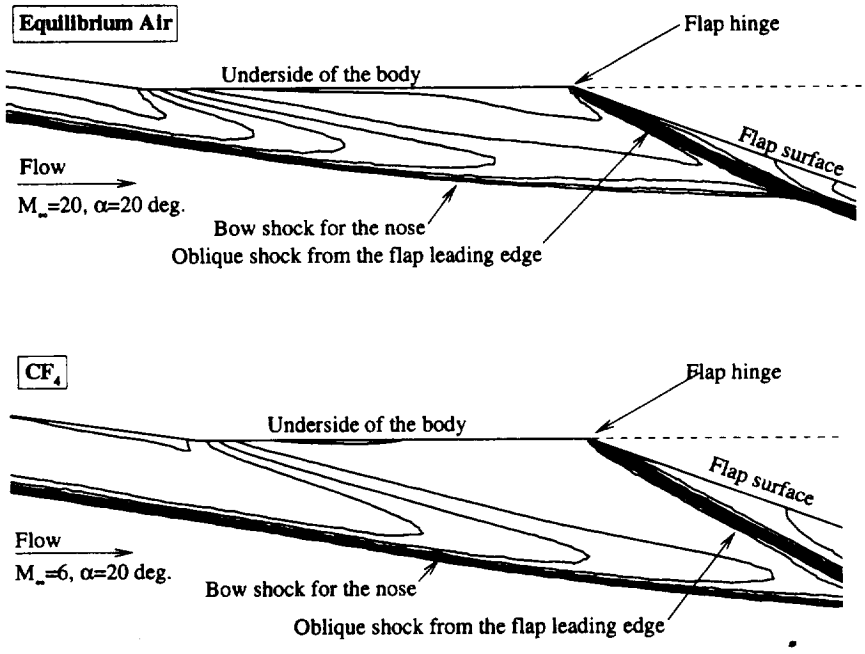

Fig. 9 Pressure contours on the symmetry plane near the flap for the 24U body in equilibrium air (M_∞=20) and CF_4 (M_∞=6) at α=20 deg.

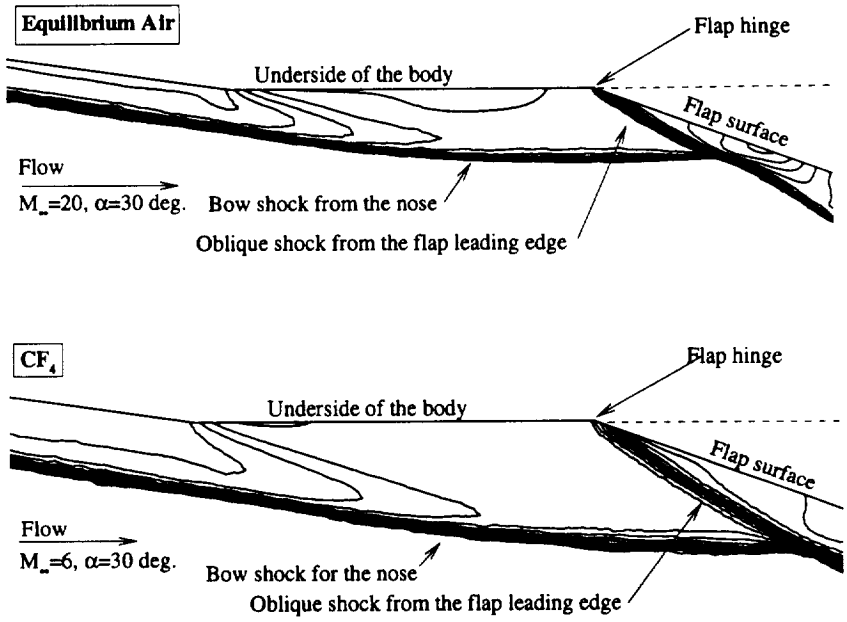

Fig. 10 Pressure contours on the symmetry plane near the flap for the 24U body in equilibrium air (M_∞=20) and CF_4 (M_∞=6) at α=30 deg.

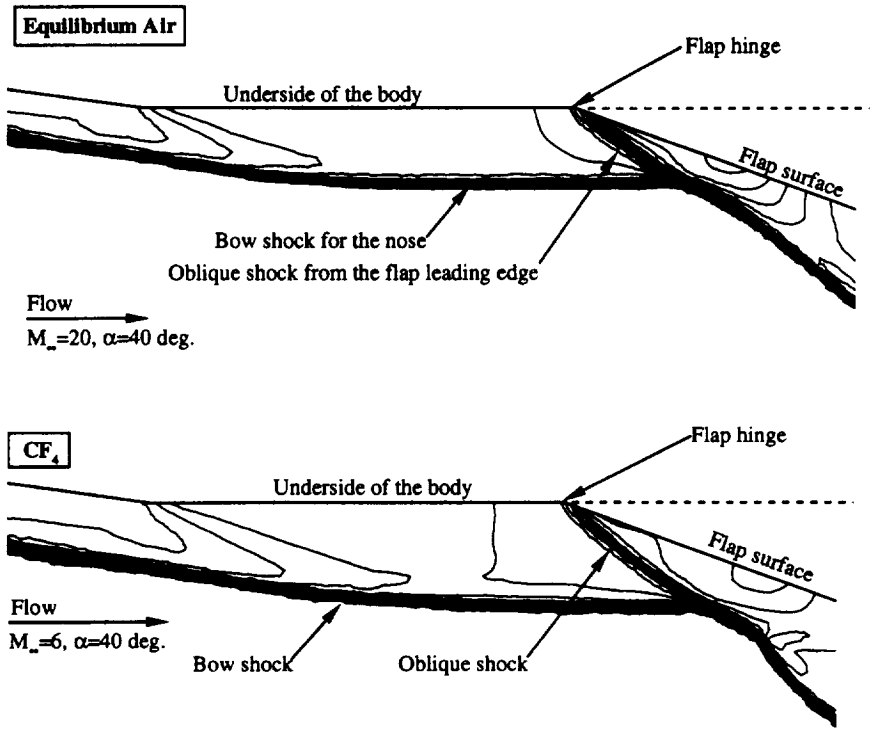

Fig. 11 Pressure contours on the symmetry plane near the flap for the 24U body in equilibrium air (M_∞=20) and CF_4 (M_∞=6) at α=40 deg.

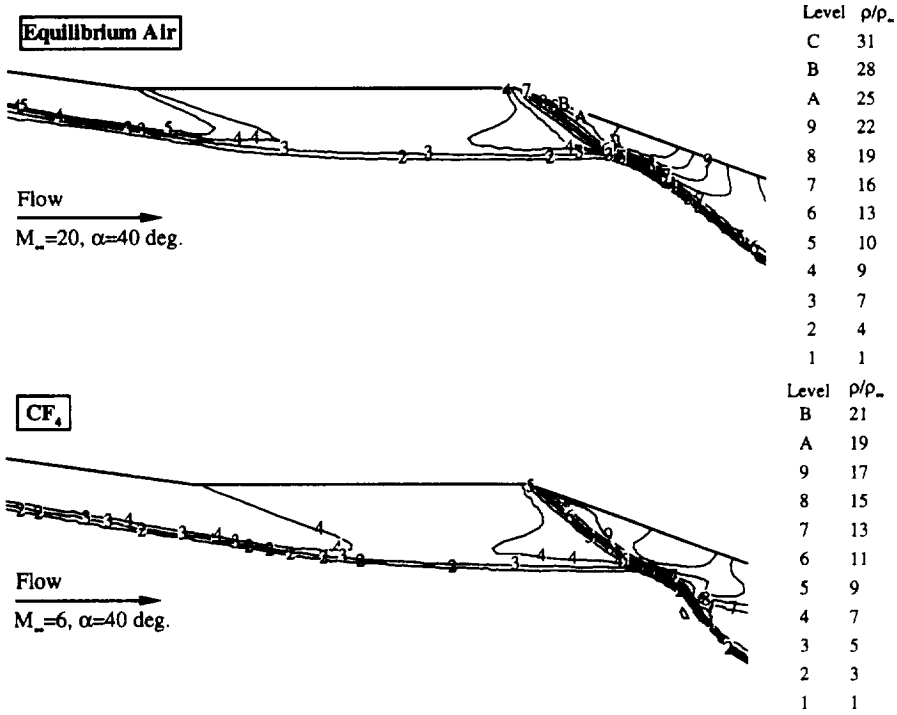

Level	ρ/ρ∞
C	31
B	28
A	25
9	22
8	19
7	16
6	13
5	10
4	9
3	7
2	4
1	1

Level	ρ/ρ∞
B	21
A	19
9	17
8	15
7	13
6	11
5	9
4	7
3	5
2	3
1	1

Fig. 12 Density contours on the symmetry plane near the flap for the 24U body in equilibrium air (M_∞=20) and CF_4 (M_∞=6) at α=40 deg.

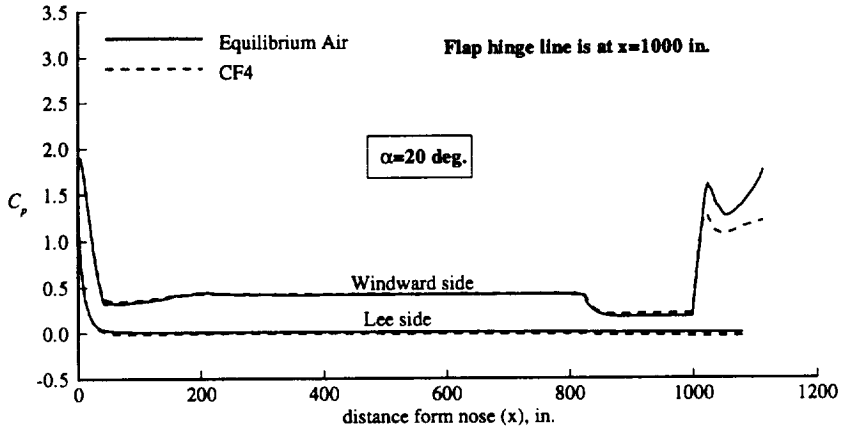

Fig. 13 Centerline Cp distributions on the 24U body in equilibrium air (M_∞=20) and CF_4 (M_∞=6) flows at α=20 deg. with 20 deg. body flap deflection

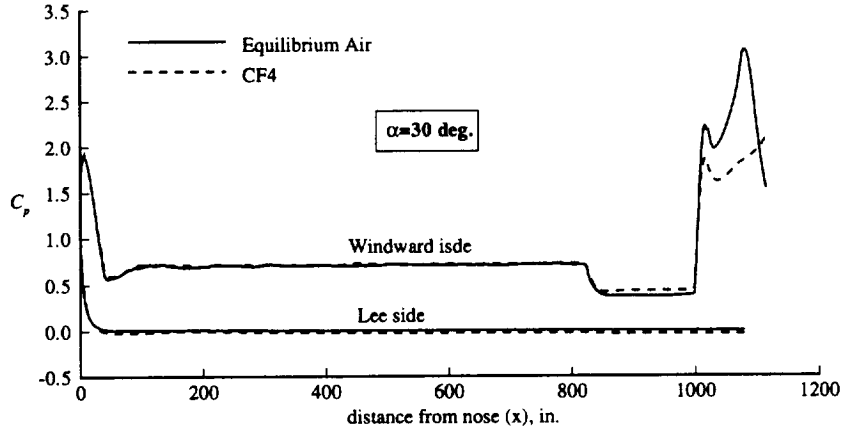

Fig. 14 Centerline C_p distributions on the 24U body in equilibrium air (M_∞=20) and CF_4 (M_∞=6) flows at α=30 deg. with 20 deg. body flap deflection

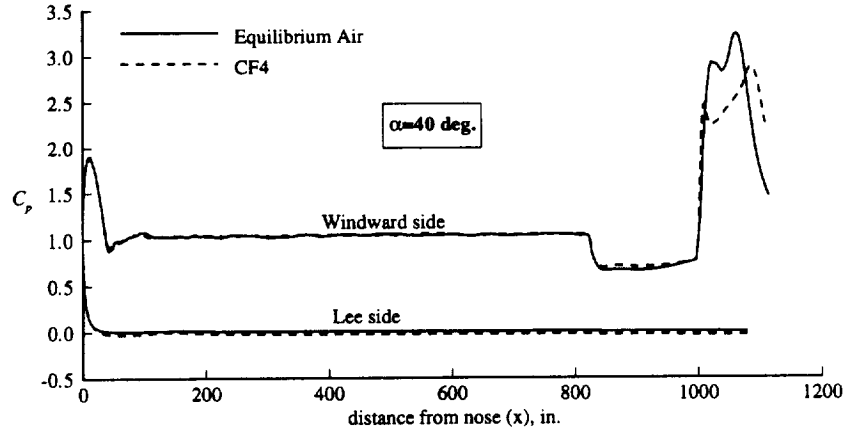

Fig. 15 Centerline C_p distributions on the 24U body in equilibrium air (M_∞=20) and CF_4 (M_∞=6) flows at α=40 deg. with 20 deg. body flap deflection

REPORT DOCUMENTATION PAGE

Form Approved
OMB No. 0704-0188

1. AGENCY USE ONLY (*Leave blank*)	2. REPORT DATE	3. REPORT TYPE AND DATES COVERED
	September 1996	Contractor Report

4. TITLE AND SUBTITLE

Computational Study of a McDonnell Douglas Single-Stage-to-Orbit Vehicle concept for Aerodynamic Analysis

5. FUNDING NUMBERS

C NAS1-19000
WU 242-20-80-02

6. AUTHOR(S)

Ramadas K. Prabhu

7. PERFORMING ORGANIZATION NAME(S) AND ADDRESS(ES)

Lockheed Martin Engineering & Sciences Company
Langley Program Office
144 Research Dr.
Hampton, VA 23666

8. PERFORMING ORGANIZATION REPORT NUMBER

9. SPONSORING/MONITORING AGENCY NAME(S) AND ADDRESS(ES)

National Aeronautics and Space Administration
Langley Research Center
Hampton, VA 23681-0001

10. SPONSORING/MONITORING AGENCY REPORT NUMBER

NASA CR-201606

11. SUPPLEMENTARY NOTES

Langley Technical Monitor: K. James Weilmuenster

12a. DISTRIBUTION/AVAILABILITY STATEMENT

Unclassified - Unlimited

Subject Category 02

12b. DISTRIBUTION CODE

13. ABSTRACT (*Maximum 200 words*)

This paper presents the results of a computational flow analysis of the McDonnell Douglas single-stage-to-orbit vehicle concept designated as the 24U. This study was made to determine the aerodynamic characteristics of the vehicle with and without body flaps over an angle of attack range of 20-40 deg. Computations were made at a flight Mach number of 20 at 200,000 ft. altitude with equilibrium air, and a Mach number of 6 with CF4 gas. The software package FELISA (Finite Element Langley Imperial College Swansea Ames) was used for all the computations. The FELISA software consists of unstructured surface and volume grid generators, and inviscid flow solvers with (1) perfect gas option for subsonic, transonic, and low supersonic speeds, and (2) perfect gas, equilibrium air, and CF4 options for hypersonic speeds. The hypersonic flow solvers with equilibrium air and CF4 options were used in the present studies. Results are compared with other computational results and hypersonic CF4 tunnel test data.

14. SUBJECT TERMS

Longitudinal Aerodynamics, Hypersonic Flow, Equilibrium Flow, Unstructured Grids

15. NUMBER OF PAGES

22

16. PRICE CODE

A03

17. SECURITY CLASSIFICATION OF REPORT	18. SECURITY CLASSIFICATION OF THIS PAGE	19. SECURITY CLASSIFICATION OF ABSTRACT	20. LIMITATION OF ABSTRACT
Unclassified	Unclassified	Unclassified	